The Design of a Novel Prismatic Drive for a Three-DOF Parallel-Kinematics Machine

Damien Chablat, Jorge Angeles

▶ **To cite this version:**

HAL Id: hal-00583260

https://hal.archives-ouvertes.fr/hal-00583260

Submitted on 5 Apr 2011

The Design of a Novel Prismatic Drive
for a Three-DOF Parallel-Kinematics Machine

D. Chablat[1], J. Angeles[2]

[1]Institut de Recherche en Communications et Cybernétique de Nantes *
UMR CNRS n° 6597, 1 rue de la Noë, 44321 Nantes, France
[2]Department of Mechanical Engineering &
Centre for Intelligent Machines, McGill University
817 Sherbrooke Street West, Montreal, Canada H3A 2K6
Damien.Chablat@irccyn.ec-nantes.fr   angeles@cim.mcgill.ca

April 7, 2011

Abstract

The design of a novel prismatic drive is reported in this paper. This transmission is based on *Slide-o-Cam*, a cam mechanism with multiple rollers mounted on a common translating follower. The design of Slide-o-Cam was reported elsewhere. This drive thus provides pure-rolling motion, thereby reducing the friction of rack-and-pinions and linear drives. Such properties can be used to design new transmissions for parallel-kinematics machines. In this paper, this transmission is intended to replace the ball-screws in Orthoglide, a three-dof parallel robot intended for machining applications.

1   Introduction

In robotics and mechatronics applications, whereby motion is controlled using a piece of software, the conversion of motion from rotational to translational is usually done by either *ball-screws* or *linear actuators*. Of these alternatives, ball-screws are gaining popularity, one of their drawbacks being the high number of moving parts that they comprise, for their functioning relies on a number of balls rolling on grooves machined on a shaft; one more drawback of ball-screws is their low load-carrying capacity, stemming from the punctual form of contact by means of which loads are transmitted. Linear bearings solve these drawbacks to some extent, for they can be fabricated with roller-bearings; however these devices rely on a form of direct-drive motor, which makes them expensive to produce and to maintain.

A novel transmission, called *Slide-o-Cam*, was introduced in [1] as depicted in Fig. 1, to transform a rotation into a translation. Slide-o-Cam is composed of four major elements: (*i*) the frame, (*ii*) the cam, (*iii*) the follower, and (*iv*) the rollers. The input axis on which the cam is mounted, the camshaft, is driven at a constant angular velocity by an actuator under computer-control. Power is transmitted to the output, the translating follower, which is the roller-carrying slider, by means of pure-rolling contact between cam and roller. The roller comprises two components, the pin and the bearing. The bearing is mounted at one end of the pin, while the other end is press-fit into the roller-carrying slider. Contact between cam and roller thus takes place at the outer surface of the bearing. The mechanism uses two conjugate cam-follower pairs, which alternately take over the motion transmission to ensure a positive action; the rollers are thus driven by the cams throughout a complete cycle. The main advantage of cam-follower mechanisms over alternative transmissions to transform rotation into translation is that contact through a roller reduces friction, contact stress and wear.

This transmission, once fully optimized, will replace the three ball-screws used by the Orthoglide prototype [2]. Orthoglide features three prismatic joints mounted orthogonaly, three identical legs and a mobile platform, which moves in Cartesian space with fixed orientation, as shown in Fig. 2. The three motors are SANYO

---

*IRCCyN: UMR n° 6597 CNRS, École Centrale de Nantes, Université de Nantes, École des Mines de Nantes

DENKI (ref. P30B08075D) with a constant torque of 1.2 Nm from 0 to 3000 rpm. This property enables the mechanism to move throughout the workspace a 4 kg load with an acceleration of 17 ms^{-2} and a velocity of 1.3 ms^{-1}. On the ball-screws, the pitch is 50 mm per cam turn. The minimum radius of the camshaft is 8.5 mm. A new arrangement of camshaft, rollers and follower is proposed to reduce the inertial load when more than two cams are used.
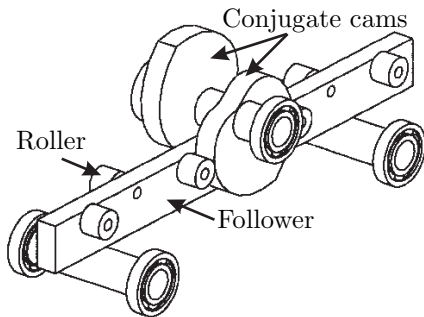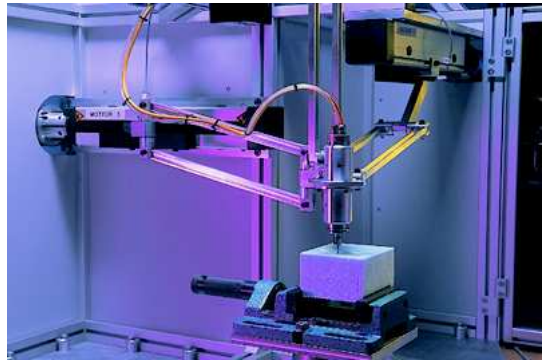

Figure 1: Layout of Slide-o-Cam

Figure 2: The Orthoglide

Unlike Lampinen [3], who used a genetic algorithm, or Zhang and Shin [4], who used what they called a relative-motion method, where the relative velocity and relative acceleration of a follower with respect to a cam is prescribed and implemented in C++, we use a deterministic method while taking into account geometric and machining constraints, as outlined in [5]. Unlike Carra [6], who used a negative-radius follower to reduce the pressure angle, we use a positive-radius follower that permits us to assemble several cams on the same roller-carrier.

In Section 2, we introduce the relations describing the cam profile and the mechanism kinematics. In Section 3, we derive conditions on the design parameters so as to have a fully convex cam profile, to avoid *undercutting*, and to have a geometrically feasible mechanism. In Section 4, the pressure angle, a key performance index of cam mechanisms, is studied in order to choose the design parameters that give the best pressure angle distribution, a compromise being made with the accuracy of the mechanism.

2 Synthesis of the Planar Cam Mechanism

Let the x-y frame be fixed to the machine frame and the u-v frame be attached to the cam, as depicted in Fig. 3. O_1 is the origin of both frames, while O_2 is the center of the roller, and C is the contact point between cam and roller. The geometric parameters defining the cam mechanism are illustrated in the same figure. The notation of this figure is based on the general notation introduced in [7], namely, (*i*) p, the pitch, *i.e.*, the distance between the center of two rollers on the same side of the follower; (*ii*) e, distance between the axis of the cam and the line of centers of the rollers; (*iii*) a_4, radius of the roller-bearing, *i.e.*, the radius of the roller; (*iv*) ψ, angle of rotation of the cam, the input of the mechanism; (*v*) s, position of the center of the roller, *i.e*, the displacement of the follower, the output of the mechanism; (*vi*) μ, pressure angle; (*vii*) **f**, force transmitted from cam to roller. In this paper, p is set to 50 mm, in order to meet the Orthoglide specifications.

The above parameters as well as the contact surface on the cam, are determined by the geometric relations dictated by the Aronhold-Kennedy Theorem in the plane [8]. When the cam makes a complete turn ($\Delta\psi = 2\pi$), the displacement of the roller is equal to p, the distance between two rollers on the same side of the roller-carrying slider ($\Delta s = p$). Furthermore, if we consider the home configuration of the roller as depicted in Fig. 4, the roller is below the x-axis for $\psi = 0$, so that we have $s(0) = -p/2$. Hence, the input-output function s is

$$s(\psi) = \frac{p}{2\pi}\psi - \frac{p}{2} \tag{1}$$

The expressions for the first and second derivatives of $s(\psi)$ with respect to ψ will be needed:

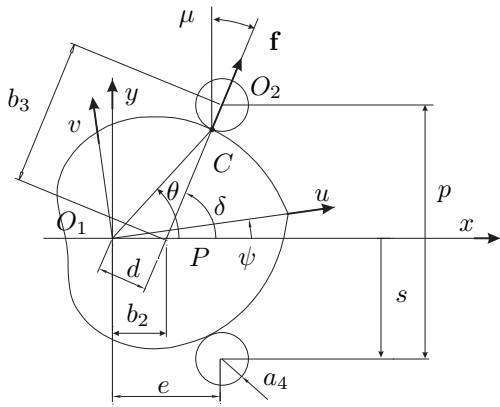$$s'(\psi) = p/(2\pi) \quad \text{and} \quad s''(\psi) = 0 \tag{2}$$
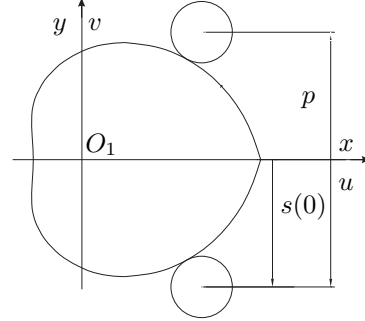
Figure 3: Parameterization of Slide-o-Cam

Figure 4: Home configuration of the mechanism

The cam profile is determined by the displacement of the contact point C around the cam. The Cartesian coordinates of this point in the u-v frame take the form [7]

$$u_c(\psi) = b_2 \cos\psi + (b_3 - a_4)\cos(\delta - \psi) \tag{3a}$$

$$v_c(\psi) = -b_2 \sin\psi + (b_3 - a_4)\sin(\delta - \psi) \tag{3b}$$

with coefficients b_2, b_3 and δ given by

$$b_2 = -s'(\psi)\sin\alpha_1 \tag{4a}$$

$$b_3 = \sqrt{(e + s'(\psi)\sin\alpha_1)^2 + (s(\psi)\sin\alpha_1)^2} \tag{4b}$$

$$\delta = \arctan\left(\frac{-s(\psi)\sin\alpha_1}{e + s'(\psi)\sin\alpha_1}\right) \tag{4c}$$

where α_1 is the directed angle between the axis of the cam and the translating direction of the follower, positive in the ccw direction. Considering the orientation adopted for the input angle ψ and for the output s, as depicted in Fig. 3, we have

$$\alpha_1 = -\pi/2 \tag{5}$$

We now introduce the nondimensional design parameter η, which will be extensively used:

$$\eta = e/p \tag{6}$$

Thus, from Eqs. (1), (2), (4a–c), (5) and (6), we find the expressions for coefficients b_2, b_3 and δ as

$$b_2 = \frac{p}{2\pi} \tag{7a}$$

$$b_3 = \frac{p}{2\pi}\sqrt{(2\pi\eta - 1)^2 + (\psi - \pi)^2} \tag{7b}$$

$$\delta = \arctan\left(\frac{\psi - \pi}{2\pi\eta - 1}\right) \tag{7c}$$

whence a first constraint on η, $\eta \neq 1/(2\pi)$, is derived. An *extended angle* Δ is introduced [9], so that the cam profile closes. Angle Δ is obtained as a root of Eq. 3. In the case of Slide-o-Cam, Δ is negative, as shown in Fig. 5. Consequently, the cam profile closes within $\Delta \leq \psi \leq 2\pi - \Delta$.

2.1 Pitch-Curve Determination

The pitch curve is the trajectory of the center O_2 of the roller, distinct from the trajectory of the contact point C, which produces the cam profile. The Cartesian coordinates of point O_2 in the x-y frame are (e, s), as
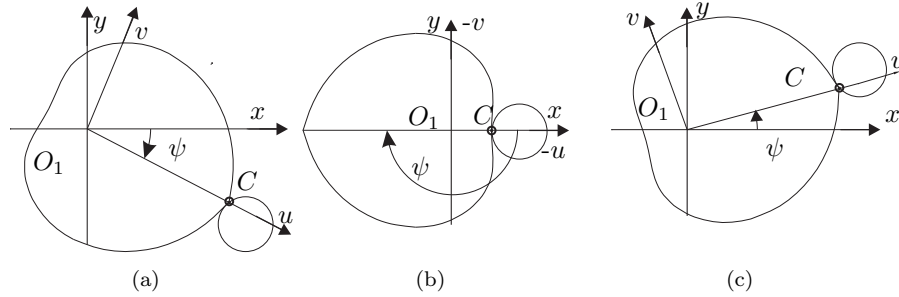
Figure 5: Orientations of the cam found when $v_c = 0$: (a) $\psi = \Delta$; (c) $\psi = \pi$; and (d) $\psi = 2\pi - \Delta$

depicted in Fig. 3. Hence, the Cartesian coordinates of the pitch-curve in the u-v frame are

$$u_p(\psi) = e\cos\psi + s(\psi)\sin\psi \tag{8a}$$
$$v_p(\psi) = -e\sin\psi + s(\psi)\cos\psi \tag{8b}$$

2.2 Geometric Constraints on the Mechanism

In order to lead to a feasible mechanism, the radius a_4 of the roller must satisfy two conditions, as shown in Fig. 6a:

- Two consecutive rollers on the same side of the roller-carrying slider must not interfere with each other. Since p is the distance between the center of two consecutive rollers, we have the constraint $2a_4 < p$. Hence the first condition on a_4:

$$a_4/p < 1/2 \tag{9}$$

- The radius b of the shaft on which the cams are mounted must be taken into consideration. Hence, we have the constraint $a_4 + b \le e$, the second constraint on a_4 in terms of the parameter η thus being

$$a_4/p \le \eta - b/p \tag{10}$$

Considering the initial configuration of the roller, as depicted in Fig. 4, the v-component of the Cartesian
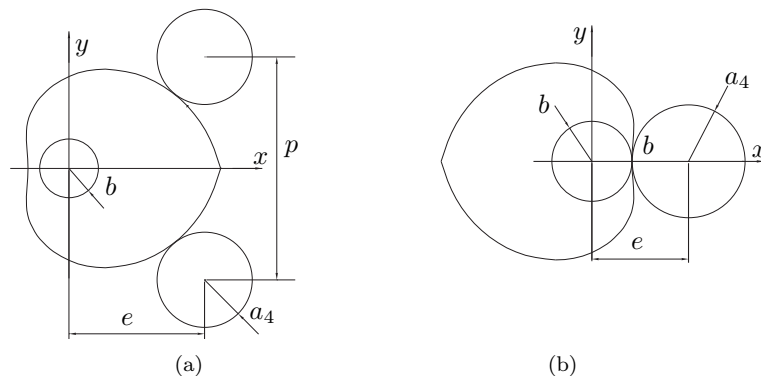
Figure 6: Constraints on the radius of the roller: (a) $a_4/p < 1/2$; and (b) $a_4/p \le \eta - b/p$.

coordinate of the contact point C is negative in this configuration, $i.e.$, $v_c(0) \le 0$. Moreover, from the expression for $v_c(\psi)$ and for parameters b_3 and δ given in Eqs. (3b), (7b & c), respectively, the above relation leads to the condition:

$$\left(\frac{p}{2\pi a_4} \sqrt{(2\pi\eta - 1)^2 + (-\pi)^2} - 1 \right) \sin\left[\arctan\left(\frac{-\pi}{2\pi\eta - 1}\right)\right] \le 0$$

Further, we define A and B as:

$$A = \frac{p}{2\pi a_4}\sqrt{(2\pi\eta - 1)^2 + \pi^2} - 1 \text{ and } B = \sin\left[\arctan\left(\frac{-\pi}{2\pi\eta - 1}\right)\right]$$

Since $(2\pi\eta - 1)^2 > 0$, we have

$$\sqrt{(2\pi\eta - 1)^2 + \pi^2} > \pi \tag{11}$$

Hence, $A > p/(2a_4) - 1$. Furthermore, from the constraint on a_4, stated in Eq. (9), we have $p/(2a_4) - 1 > 0$, whence $A > 0$. Consequently, the constraint $v_c(0) \leq 0$ leads to the constraint $B \leq 0$. We rewrite the constraint B, by using the trigonometric relation,

$$\forall x \in \mathbb{R}, \ \ \sin(\arctan x) = \frac{x}{\sqrt{1 + x^2}}$$

Hence the constraint $v_c(0) \leq 0$ becomes

$$B \leq 0 \iff \frac{-\pi}{(2\pi\eta - 1)\sqrt{1 + \pi^2/(2\pi\eta - 1)^2}} \leq 0$$

which holds only if $2\pi\eta - 1 > 0$. Finally, the constraint $v_c(0) \leq 0$ leads to a constraint on η, namely,

$$\eta > 1/(2\pi) \tag{12}$$

2.3 Pressure Angle

The pressure angle is defined as the angle between the common normal at the cam-roller contact point C and the velocity of the follower [10], as depicted in Fig. 3, where the presure angle is denoted by μ. The smaller $|\mu|$, the better the force transmission. In the case of high-speed operations, *i.e.*, angular velocities of cams exceeding 50 rpm, the recommended bounds of the pressure angle are within $30°$. Nevertheless, as it is not always possible to have a pressure angle that remains below $30°$, we adopt the concept of *service factor*, which is the percentage of the working cycle with a pressure angle within $30°$ [9]. The service angle will be useful to take into consideration these notions in the ensuing discussion, when optimizing the mechanism.

For the case at hand, the expression for the pressure angle μ is given in [10] as

$$\mu = \arctan\left(\frac{s'(\psi) - e}{s(\psi)}\right)$$

Considering the expressions for s and s', and using the parameter η given in Eqs. (1), (2a) and (6), respectively, the expression for the pressure angle becomes

$$\mu = \arctan\left(\frac{1 - 2\pi\eta}{\psi - \pi}\right) \tag{13}$$

We are only interested in the value of the pressure angle with the cam driving the roller, which happens with

$$\pi \leq \psi \leq 2\pi - \Delta \tag{14}$$

Indeed, if we start the motion in the home configuration depicted in Fig. 4, with the cam rotating in the ccw direction, the cam begins to drive the roller only when $\psi = \pi$; and the cam can drive the follower until contact is lost, *i.e.*, when $\psi = 2\pi - \Delta$, as shown in Figs. 5b & c.

Nevertheless, as shown in Fig. 7, the conjugate cam can also drive the follower when $0 \leq \psi \leq \pi - \Delta$; there is therefore a common interval, for $\pi \leq \psi \leq \pi - \Delta$, during which two cams can drive the follower. In this interval, the conjugate cam can drive a roller with lower absolute values of the pressure angle. We assume that, when the two cams can drive the rollers, the cam with the lower absolute value of pressure angle effectively drives the follower. Consequently, we are only interested in the value of the pressure angle in the interval,

$$\pi - \Delta \leq \psi \leq 2\pi - \Delta \tag{15}$$

We study here the influence of parameters η and a_4 on the values of the pressure angle while the cam drives the roller, *i.e.*, with $\pi - \Delta \leq \psi \leq 2\pi - \Delta$, as explained above.

- *Influence of parameter η*: Figure 8 shows the influence of the parameter η on the pressure angle, with a_4 and p being fixed. From these plots we have one result: *The lower η, the lower $|\mu|$*.

- *Influence of the radius of the roller a_4*: a_4 does not appear in the expression for the pressure angle, but it influences the value of the extended angle Δ, and hence, the plot boundaries of the pressure angle, as shown in Fig. 7.

By computing the value of the extended angle Δ for several values of a_4, we can see that the higher a_4, the lower $|\Delta|$. Consequently, since the boundaries to plot the pressure angle are $\pi - \Delta$ and $2\pi - \Delta$, we can see that when we increase a_4, $-\Delta$ decreases and the boundaries are translated toward the left, *i.e.*, toward higher absolute values of the pressure angle.
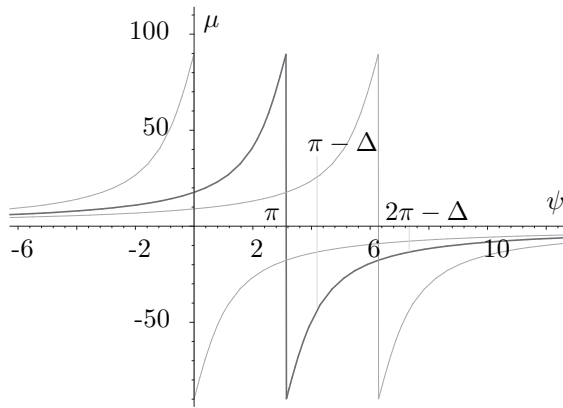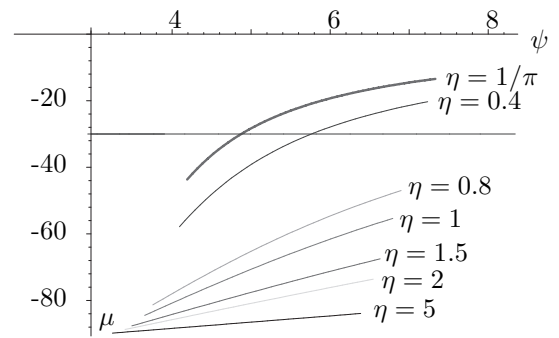

Figure 7: Pressure angle distribution

Figure 8: Influence of parameter η on the pressure angle μ (in degree), with $p = 50$ mm and $a_4 = 10$ mm

3 Convexity of the Cam Profile and Undercutting

In order to enhance machining accuracy, we need the cam profile to be fully convex. In this section we establish conditions on the design parameters η and a_4 in order to have a fully convex cam profile. We thus study the sign-change in the curvature of the cam profile via that of the pitch curve. Furthermore, for cam design in roller-follower mechanisms, we should also consider *undercutting*. Undercutting occurs when the radius of the roller is greater than or equal to the minimum absolute value of the radius of curvature of the pitch curve. Upon avoiding undercutting, the sign of the curvature of the pitch curve is identical to that of the cam profile.

3.1 Curvature of the Cam Profile

The curvature of any planar parametric curve, in terms of the Cartesian coordinates u and v, and parameterized with any parameter ψ, is given by [10]:

$$\kappa = \frac{v'(\psi)u''(\psi) - u'(\psi)v''(\psi)}{[u'(\psi)^2 + v'(\psi)^2]^{3/2}} \tag{16}$$

The sign of κ in Eq. (16) tells whether the curve is convex or concave at a point: a positive κ implies convexity, while a negative κ implies concavity at that point. To obtain the curvature of the cam profile for a given roller-follower, we use the Cartesian coordinates of the pitch curve, since obtaining its first and second derivatives leads to simpler expressions as compared with those associated with the cam profile itself. Then, the curvature of the cam profile is derived by a simple geometric relationship between the curvatures of the pitch curve and of the cam profile.

The Cartesian coordinates of the pitch curve were recalled in Eqs. (8a & b), while Eqs. (2a & b) give their first and second derivatives as

$$s(\psi) = p/(2\pi)\psi - p/2 , \quad s'(\psi) = p/(2\pi) , \quad s''(\psi) = 0$$

With the above-mentioned expressions, we can compute the first and second derivatives of the Cartesian coordinates of the pitch curve with respect to the angle of rotation of the cam, ψ:

$$u_p'(\psi) \;=\; [s'(\psi) - e]\sin\psi + s(\psi)\cos\psi \tag{17a}$$

$$v_p'(\psi) \;=\; [s'(\psi) - e]\cos\psi - s(\psi)\sin\psi \tag{17b}$$

$$u_p''(\psi) \;=\; [2s'(\psi) - e]\cos\psi - s(\psi)\sin\psi \tag{17c}$$

$$v_p''(\psi) \;=\; -[2s'(\psi) - e]\sin\psi - s(\psi)\cos\psi \tag{17d}$$

By substituting $\eta = e/p$, along with Eqs. (17a–d), into Eq. (16), the curvature κ_p of the pitch curve is obtained as

$$\kappa_p = \frac{2\pi}{p}\,\frac{[(\psi - \pi)^2 + 2(2\pi\eta - 1)(\pi\eta - 1)]}{[(\psi - \pi)^2 + (2\pi\eta - 1)^2]^{3/2}} \tag{18}$$

which remains bounded by virtue of condition (12).

Let ρ_c and ρ_p be the radii of curvature of both the cam profile and the pitch curve, respectively, and κ_c the curvature of the cam profile. Since the curvature is the reciprocal of the radius of curvature, we have $\rho_c = 1/\kappa_c$ and $\rho_p = 1/\kappa_p$. Furthermore, due to the definition of the pitch curve, it is apparent that

$$\rho_p = \rho_c + a_4 \tag{19}$$

Writing Eq. (19) in terms of κ_c and κ_p, we obtain the curvature of the cam profile as

$$\kappa_c = \frac{\kappa_p}{1 - a_4\kappa_p} \tag{20}$$

with κ_p given in Eq. (18). As we saw previously, we want the cam profile to be fully convex, which happens if the pitch curve is fully convex too. We thus find first the convexity condition of the pitch curve.

3.2 Convexity Condition of the Pitch Curve

Considering the expression for κ_p in Eq. (18), we have, for every value of ψ, $\kappa_p \geq 0$ if $(2\pi\eta - 1)(\pi\eta - 1) \geq 0$ and $\eta \neq 1/(2\pi)$, whence the condition on η:

$$\kappa_p \geq 0 \quad \text{if} \quad \eta \in [0, 1/(2\pi)[\;\; \cup \;\; [1/\pi, +\infty[\tag{21}$$

Figure 9 shows pitch-curve profiles and their curvatures for two values of η. The condition on η given in Eq. (21)
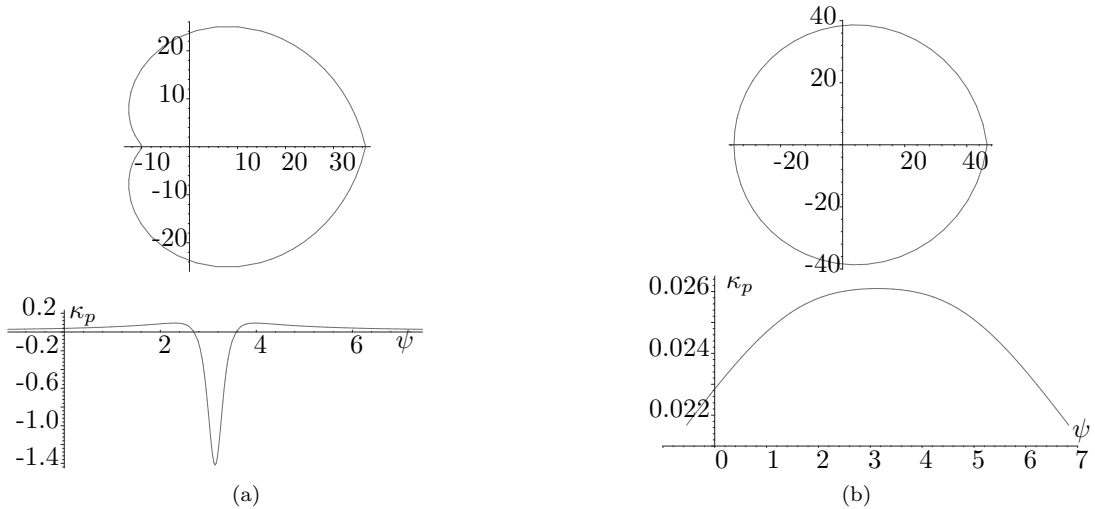

Figure 9: Pitch-curve profiles and their corresponding curvatures with $p = 50$ mm:
(a) $\eta = 0.2$ ($\eta \in]1/(2\pi), 1/\pi[$) and (b) $\eta = 0.7$ ($\eta > 1/\pi$)

must be combined with the condition appearing in Eq. (12), $\eta > 1/(2\pi)$; hence, the final **convexity condition of the pitch curve** is:

$$\eta \geq 1/\pi \tag{22}$$

3.3 Undercutting-Avoidance

We assume in this subsection that the pitch curve is fully convex, *i.e.*, $\kappa_p \geq 0$ and $\eta \geq 1/\pi$. In order to avoid undercutting, *i.e.*, in order to have both the cam profile and the pitch curve fully convex, we need κ_c to be positive. Considering the expression for the curvature of the cam profile κ_c of Eq. (20), the condition to avoid undercutting is $1 - a_4\kappa_p > 0$, whence the condition on the radius of the follower a_4:

$$a_4 < \frac{1}{\kappa_p(\psi)} \qquad \forall\ \psi \in \mathbb{R}$$

Since κ_p is positive, this condition can be written as

$$a_4 < \frac{1}{\kappa_{p\max}} \quad , \quad \text{with} \quad \kappa_{p\max} = \max_{\psi \in \mathbb{R}} \kappa_p(\psi) \tag{23}$$

- *Expression for $\kappa_{p\max}$*: In order to compute the expression for $\kappa_{p\max}$, we need the first derivative κ_p' of κ_p with respect to ψ and its roots. With the condition $\eta \geq 1/\pi$, the expression for κ_p given in Eq. (18) is differentiable for every value of ψ. We thus obtain

$$\kappa_p' = -\frac{2\pi}{p} \frac{(\psi - \pi)(\psi^2 - 2\pi\psi + \pi^2 + 4\eta^2\pi^2 - 10\eta\pi + 4)}{[(\psi - \pi)^2 + (2\pi\eta - 1)^2]^{5/2}} \tag{24}$$

The roots of κ_p' are, apparently, $\psi_1 = \pi$ and the roots ψ_2 and ψ_3 of the polynomial

$$P(\psi) = \psi^2 - 2\pi\psi + \pi^2 + 4\eta^2\pi^2 - 10\eta\pi + 4$$

Let β_ψ be the discriminant of the equation $P = 0$, *i.e.*,

$$\beta_\psi = -4\eta^2\pi^2 + 10\eta\pi - 4$$

Therefore, the sign of β_ψ and, consequently, the roots ψ_2 and ψ_3, depend on the value of η. Let β_η be the discriminant of $\beta_\psi = 0$, a quadratic equation in η. Hence, $\beta_\eta = 9\pi^2$, which is positive. The two roots of β_ψ are $1/2\pi$ and $2/\pi$. Thus,

$$\beta_\psi > 0 \quad \text{if} \quad \eta \in \left[\frac{1}{\pi}, \frac{2}{\pi}\right[\quad \text{or} \quad \beta_\psi < 0 \ \text{ if } \ \eta \in \left]\frac{2}{\pi}, +\infty\right[$$

$$\beta_\psi = 0 \quad \text{if} \quad \eta = \frac{2}{\pi}$$

We now study the roots of κ_p' according to the value of η.

- $\eta \in [1/\pi, 2/\pi[$: $\beta_\psi > 0$, and the polynomial P has two roots ψ_2 and ψ_3, so that κ_p' has three roots:

$$\psi_1 = \pi \tag{25a}$$
$$\psi_2 = \pi + \sqrt{-4\eta^2\pi^2 + 10\eta\pi - 4} \tag{25b}$$
$$\psi_3 = \pi - \sqrt{-4\eta^2\pi^2 + 10\eta\pi - 4} \tag{25c}$$

- $\eta \in]2/\pi, +\infty[$: $\beta_\psi < 0$, and the polynomial P has no real roots, so that κ_p' has only one root, $\psi_1 = \pi$.

- $\eta = 2/\pi$: $\beta_\psi = 0$, and the polynomial P has one double root equal to π, so that κ_p' has one triple root $\psi_1 = \pi$.

To decide whether these roots correspond to minima or maxima, we need to know the sign of the second derivative κ_p'' of κ_p with respect to ψ, for the corresponding values of ψ. If the second derivative is negative, the stationary value is a maximum; if positive, a minimum. The expressions for the second derivatives, as derived with computer algebra, for the values of ψ given in Eqs. (25a–c):

$$\kappa_p''(\psi_1) = \frac{4\pi(\eta\pi - 2)}{p|2\eta\pi - 1|^3(2\eta\pi - 1)} \qquad \kappa_p''(\psi_2) = \kappa_p''(\psi_3) = \frac{8\pi(\eta\pi - 2)}{9p(2\eta\pi - 1)\sqrt{6\eta\pi - 3}}$$
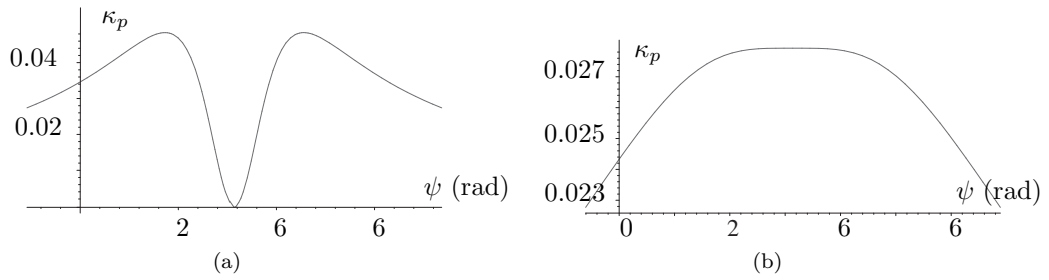
Figure 10: Pitch-curve curvature for $p = 50$ mm: (a) $\eta = 1/\pi$ and (b) $\eta = 2/\pi$

- If $\eta \in [1/\pi, 2/\pi[$, $\kappa_p''(\psi_1) > 0$ and $\kappa_p''(\psi_2) = \kappa_p''(\psi_3) < 0$, the curvature of the pitch curve has one local minimum for ψ_1 and two maxima, for ψ_2 and ψ_3. Hence, the value of $\kappa_{p\max}$ is

$$\kappa_{p\max1} = \kappa_p(\psi_2) = \kappa_p(\psi_3) = \frac{4\pi}{3p\sqrt{6\eta\pi - 3}} \tag{26}$$

  Figure 10a shows a plot of the pitch-curve curvature with $\eta = 1/\pi$ and $p = 50$ mm. Since η is taken equal to the convexity limit $1/\pi$, the curvature remains positive and only vanishes for $\psi = \pi$.

- If $\eta \in]2/\pi, +\infty[$, $\kappa_p''(\psi_1) < 0$, the curvature of the pitch curve has a maximum for ψ_1. Hence, the value of $\kappa_{p\max}$ is

$$\kappa_{p\max2} = \kappa_p(\psi_1) = \frac{4\pi}{p} \frac{(2\eta^2\pi^2 - 3\eta\pi + 1)}{(4\eta^2\pi^2 - 4\eta\pi + 1)^{3/2}} \tag{27}$$

  Figure 9d shows a plot of the pitch-curve curvature with $\eta = 0.7$ ($\eta > 2/\pi$) and $p = 50$ mm.

- If $\eta = 2/\pi$, $\kappa_p''(\psi_1) = 0$, we cannot tell whether we are in the presence of a maximum or a minimum. We solve this uncertainty graphically, by plotting the curvature of the pitch curve for $\eta = 2/\pi$ and $p = 50$ mm. Figure 10b reveals that the curvature has a maximum for ψ_1. The value of this maximum can be obtained by substituting η by $2/\pi$ into either $\kappa_{p\max1}$ or $\kappa_{p\max2}$, expressed in Eqs. (26) and (27), respectively.

In summary, to have a fully convex cam profile, taking the geometric constraints on the mechanism into consideration, parameter η must obey the condition given in Eq. (22), *i.e.* $\eta \geq 1/\pi$. We combine the condition on a_4 to avoid undercutting, as given in Eq. (23), with the geometric constraints on the mechanism, as given in Eqs. (9) and (10), which are, respectively, $a_4/p < 1/2$ and $a_4/p \leq \eta - b/p$:

$$\text{if } \eta \in \left[\frac{1}{\pi}, \frac{2}{\pi}\right], \quad a_4 \;<\; \min\left\{\frac{1}{\kappa_{p\max1}}, \; \frac{p}{2}, \; \eta p - b\right\} \tag{28a}$$

$$\text{if } \eta \in \left[\frac{2}{\pi}, +\infty\right[, \quad a_4 \;<\; \min\left\{\frac{1}{\kappa_{p\max2}}, \; \frac{p}{2}, \; \eta p - b\right\} \tag{28b}$$

where $\kappa_{p\max1}$ and $\kappa_{p\max2}$ are given in Eqs. (26) and (27), respectively.

4 Optimization of the Roller Pin

We concluded in the previous section that the lowest values of parameters η and a_4 led to the lowest values of the pressure angle. Nevertheless, we must take into consideration that the smaller the radius of the roller, the bigger the deformation of the roller pin, and hence, a decrease of the stiffness and the accuracy of the mechanism. In this section we formulate and solve an optimization problem to find the best compromise on parameters η and a_4 to obtain the lowest pressure angle values with an acceptable deformation of the roller pin. In this section we adopt the approach proposed by Teng and Angeles [11].

4.1 Minimization of the Elastic Deformation on the Roller Pins

Here we find the expression for the maximum elastic deformation on the pin, which will be minimized under given constraints. Figure 11 displays the free part of the pin, *i.e.*, the part not fixed to the roller-carrying slider, as a cantilever beam, where the load $F = \sqrt{f_x^2 + f_y^2}$ denotes the magnitude of the force $\mathbf{f}$ transmitted by the cam. This force is applied at a single point at the end of the pin in the worst loading case. Although the dimensions of the pin are not those of a simple beam, we assume below that the pin can be modeled as such, in order to obtain an explicit formula for its deflection. This assumption was found to be plausible by testing it with FEA [11].
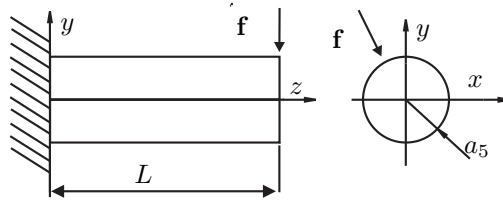

Figure 11: Approximation of the roller pin as a cantilever beam

The displacement v_L at the free end of the pin turns out to be

$$v_L = \sqrt{v_x^2 + v_y^2} = \frac{FL^3}{3EI} \tag{29}$$

where E is the Young modulus and $I = \pi a_5^4/4$, with a_5 denoting the radius of the pin, is the polar moment of inertia of the cross section. Moreover, v_x and v_y are the pin elastic displacements in the x- and y-directions, respectively, at the free end.

Before proceeding, we prove that the vertical component f_y of the transmitted force is constant, and hence, we will consider only the magnitude of the x-component of v_L. Since we assume that the mechanism undergoes a pure-rolling motion, the force exerted by the cam onto the roller, denoted by $\mathbf{f} = [f_x \ f_y]^T$, passes through the center of the roller, *i.e.*, its line of action passes through points O_2 and C, as depicted in Fig. 3. With a constant torque τ provided by the motor, we have $\tau = ||\mathbf{f}||d$, where d denotes the distance from the center of the input axis to the line of action of the force $\mathbf{f}$. Moreover, we have $d = b_2 \sin \delta$. Hence, $\tau = ||\mathbf{f}||(b_2 \sin \delta) = b_2(||\mathbf{f}|| \sin \delta) = b_2 f_y$. Finally, since $b_2 = 2\pi/p$ we obtain the expression for f_y sought:

$$f_y = \frac{2\pi\tau}{p} = F_0 \tag{30}$$

Since τ is constant, f_y is also constant throughout one full turn of the cam. Consequently we only have to consider the x-component of $\mathbf{f}$, and hence, v_x, as given below, should be minimized:

$$v_x = \frac{|f_x|L^3}{3EI} = \frac{4|f_x|L^3}{3E\pi a_5^4} = \beta \frac{|f_x|}{a_5^4}, \quad \beta = \frac{4L^3}{3E\pi} \tag{31}$$

β thus being a constant factor. The objective function z, to be minimized, is thus defined as

$$z = \frac{f_{\max}^2}{a_5^4} \quad \rightarrow \quad \min_{\eta, a_4, a_5} \tag{32}$$

where $f_{\max}$ is the maximum value of f_x throughout one cycle. Since

$$f_x = \frac{f_y}{\tan \delta} = \frac{F_0}{\tan \delta} \tag{33}$$

we obtain

$$z = \frac{1}{a_5^4} \max_\psi \left\{ f_x^2 \right\} = \frac{1}{a_5^4} \max_\psi \left\{ \frac{F_0^2}{\tan^2 \delta} \right\} = \frac{F_0^2}{a_5^4} \max_\psi \left\{ \frac{1}{\tan^2 \delta} \right\}$$

with δ, a function of ψ, given in Eq. (7c). Moreover, the system operates by means of two conjugate mechanisms, which alternately take over the power transmission. We established in Eq. (15) that when one mechanism is in positive action, ψ is bounded between $\psi_i = \pi - \Delta$ and $\psi_f = 2\pi - \Delta$, which corresponds to δ bounded between δ_i and δ_f with $0 \le \delta_i < \delta_f \le \pi$. Moreover, functions $1/\tan^2 \delta$ and $\cos^2 \delta$ are both unimodal in $-\pi \le \delta \le 0$ and in $0 \le \delta \le \pi$, their common maxima finding themselves at $-\pi$, 0 and π. Since $\cos^2 \delta$ is better behaved than $1/\tan^2 \delta$, we redefine z as

$$z = \frac{1}{a_5^4} \max_{\delta_i \le \delta \le \delta_f} \left\{ \cos^2 \delta \right\}$$

Furthermore, the function $\cos^2 \delta$ attains its global minimum of 0 in $[0, \ \pi]$, its maximum in the interval $[\delta_i, \ \delta_f]$, included in $[0, \ \pi]$, occurring at the larger of the two extremes of the interval, δ_i or δ_f. It follows that the objective function to be minimized becomes

$$z = \frac{1}{a_5^4} \max \left\{ \cos^2 \delta_i, \ \cos^2 \delta_f \right\} \longrightarrow \min_{\nu, a_4, a_5}$$

with δ_i and δ_f the values of δ for $\psi_i = \pi - \Delta$ and $\psi_f = 2\pi - \Delta$, respectively. Using the expression for δ given in Eq. (7c) and the trigonometric identity

$$\cos(\arctan x) = \frac{1}{\sqrt{1+x^2}}$$

we obtain the expression for $\cos^2 \delta$:

$$\cos^2 \delta = \frac{(2\pi\eta - 1)^2}{(2\pi\eta - 1)^2 + (\psi - \pi)^2} \tag{34}$$

Hence,

$$\cos^2 \delta_i \ = \ \frac{(2\pi\eta - 1)^2}{(2\pi\eta - 1)^2 + (\psi_i - \pi)^2} \tag{35a}$$

$$\cos^2 \delta_f \ = \ \frac{(2\pi\eta - 1)^2}{(2\pi\eta - 1)^2 + (\psi_f - \pi)^2} \tag{35b}$$

Furthermore, since $\psi_i = \pi - \Delta$, $\psi_f = 2\pi - \Delta$ and $\Delta < 0$, we have $\psi_f > \psi_i > \pi$, $\psi_f - \pi > \psi_i - \pi > 0$ and, consequently, from Eqs. (35a & b), $\cos^2 \delta_i > \cos^2 \delta_f$ and the objective function to minimize becomes

$$z = \frac{\cos^2 \delta_i}{a_5^4} \quad \rightarrow \quad \min_{\eta, a_4, a_5} \tag{36}$$

with $\cos^2 \delta_i$ given in Eq. (35a) and $\psi_i = \pi - \Delta$.

4.2   Geometric Constraints

Two neighboring pins cannot be tangent to each other, as depicted in Fig. 12, and hence the radius a_5 of the pin is bounded as

$$a_5/p < 1/4 \tag{37}$$

Furthermore, a_4 and a_5 are not independent. From the SKF catalogue, for example, we have information on bearings available in terms of the outer radius D and the inner radius d, as shown in Fig. 13. We divide these bearings into five series, from 1 to 5. Hence, each series can be represented by a continuous function. We chose series 2, in which the basic dynamic load rating C lies between 844 and 7020 N. Furthermore, for series 2, the relation between D and d can be approximated by a linear function D vs. d, $D \simeq 1.6d + 10$ (in mm). Since $D = 2a_4$ and $d = 2a_5$, the above equation leads to
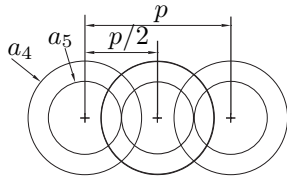
$$a_4 \simeq 1.6a_5 + 5 \quad \text{in mm} \tag{38}$$
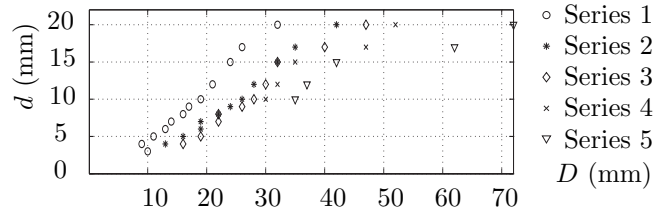
Figure 12: Geometric constraint on the roller-pin radius

Figure 13: Dimensions of the SKF bearings

We define now two non-dimensional parameters α_4 and α_5:

$$\alpha_4 = a_4/p \qquad \alpha_5 = a_5/p \tag{39}$$

where α_5 can be derived from Eq. (38) as

$$\alpha_5 = (5/8)\alpha_4 - 25/(8p) \quad \text{with } p \text{ in mm.} \tag{40}$$

Moreover, we recall the geometric constraint defined in Eqs. (22) and (28) which can be rewritten as

$$g_1 = \frac{1}{\pi} - \eta \leq 0 \tag{41a}$$

$$g_2 = \alpha_4 - \frac{1}{2} < 0 \tag{41b}$$

$$g_3 = \alpha_4 - \frac{1}{p\kappa_{p\max}} < 0 \tag{41c}$$

$$g_4 = \alpha_4 - \eta + \frac{b}{p} \leq 0 \tag{41d}$$

$$g_5 = \alpha_5 - \frac{1}{4} < 0 \tag{41e}$$

with $\cos^2 \delta_i$ and α_5 given in Eqs. (35a) and (40), respectively.

4.3   Results of the Optimization Problem

We solve the foregoing optimization problem using the $fmincon$ function of Matlab which is base on semi quadratic programming, using $p = 50$ mm and $b = 9.5$ mm. One solution is found, corresponding to $\eta = 0.69$ and $a_4 = 24.9992$ mm, with a value of $z = 249$. The algorithm finds the values of η and a_4 as big as possible considering the constraints. For this solution, constraints (41d & e) are active. Nevertheless, as we saw in Subsection 3.3. about the influence of parameters h and a_4, we want these parameters to be as small as possible in order to have low pressure angle values. For the solution found above, the service factor is equal to 0%. Consequently, we must find a compromise between the pressure angle and the roller-pin elastic deformation. Table 1 shows solutions found by the optimization algorithm upon reducing the boundaries of η. Each time the algorithm finds the corresponding value of a_4 as big as possible, constraint (41d) becomes active. Recorded in this table is also the corresponding maximum elastic deformation of the roller pin $v_{L\max}$ (its expression is derived below), the minimum and the maximum absolute values of the pressure angle, $|\mu_{\min}|$ and $|\mu_{\max}|$, respectively, and the service factor, as defined in Section 2.4. From Eqs. (29) and (31) we have

$$v_L = \frac{\beta}{a_5^4}\sqrt{f_x^2 + f_y^2}$$

Using Eqs. (30) and (33), the above equation leads to

$$v_L = \frac{\beta F_0}{a_5^4}\sqrt{1 + \frac{1}{\tan^2 \delta}}$$

which can be simplified by means of the expression for $\cos^2 \delta_i$ given in Eq. (35a) as

$$v_{L\max} = \frac{\beta F_0}{a_5^4} \frac{\sqrt{(2\pi\eta - 1)^2 + (\psi_i - \pi)^2}}{|\psi_i - \pi|} \tag{42}$$

with F_0, β and a_5 given in Eqs. (30), (31) and (38), respectively, and $\psi_i = \pi - \Delta$. In Table 1 we record the value of $v_{L\max}$ with $L = 10$ mm, $\tau = 1.2$ Nm (according to the Orthoglide specifications recalled in Section 1) and $E = 2 \times 10^5$ MPa. We conclude from Table 1 that for this cam profile we cannot find an acceptable compromise between a low deformation of the roller pin, and hence a high stiffness and accuracy of the mechanism, and low pressure angle values. Indeed, for an acceptable deformation of the roller pin, $v_{L\max} = 8.87$ μm, obtained with $\eta = 0.38$, the service factor equals 54.68%, which is too low. On the other hand, for an acceptable service factor of 79.43%, obtained with $\eta = 1/\pi \approx 0.3183$, the deformation of the roller pin is equal to 710.19 μm, which is too high.

Figure 14 depicts a rapid protote of the optimum mechanism whith an intermediate value, namely, $\eta = 0.35$. The motor and the two cams translate, while the follower and the rollers stay fixed on the base.

η	a_4 (mm)	a_5 (mm)	z	$v_{L\max}$ (μm)	$|\mu_{\min}|$ (°)	$|\mu_{\max}|$ (°)	service factor (%)
0.69	24.99	12.50	249	0.09	42.11	80.68	0
0.5	15.5	6.56	2968	0.50	28.59	69.81	6.85
0.4	10.5	3.44	32183	4.32	20.31	57.99	46.68
0.39	10	3.12	45490	6.07	19.46	56.42	50.68
0.38	9.5	2.81	66659	8.87	18.61	54.78	54.68
0.37	9	2.50	102171	13.63	17.75	53.04	58.69
0.36	8.5	2.19	165896	22.31	16.89	51.22	62.69
0.35	8	1.87	290765	39.71	16.03	49.31	66.70
0.34	7.5	1.56	566521	79.18	15.17	47.31	70.72
0.33	7	1.25	$1.29 \ 10^6$	186.06	14.31	45.21	74.73
$1/\pi$	6.41	0.88	$4.68 \ 10^6$	710.19	13.31	42.64	79.43

Table 1: Results of the optimization problem, with $p = 50$ mm, $b = 9.5$ mm, $L = 10$ mm, $\tau = 1.2$ Nm and $E = 2 \times 10^5$ MPa
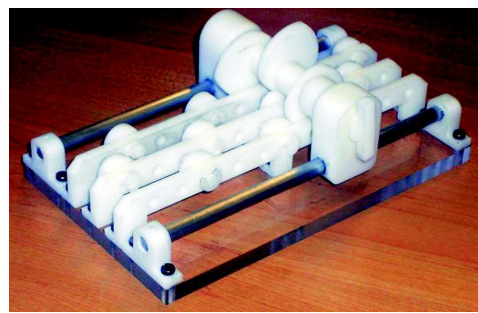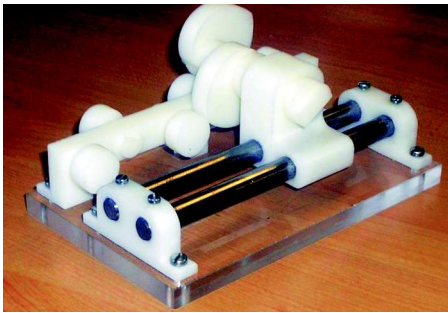
Figure 14: Layout of the two coaxial conjugate-cam mechanism on the same shaft

Figure 15: Layout of the three conjugate-cam mechanism on the same shaft

5 Novel Conjugate-Cam Mechanism

This Section describes a novel mechanism and its prototype, based on Slide-o-Cam, that enables us to decrease considerably the pressure angle while meeting the Orthoglide specifications.

This mechanism is composed of three conjugate cams mounted either (*i*) on three parallel shafts (with the rollers placed on one single side of the roller-carrier) or (*ii*) on a single shaft (with the rollers placed on

one single side of three parallel roller-carrier), as depicted in Fig. 15. Mounted on two guideways, one motor provides the torque to one camshaft. In case (i), the torque is transmitted to the two other camshafts through a parallelogram mechanism coupling them, whose detailed design is reported in [12]. Shown in Fig. 16 is a layout of this case, with 1, 2 and 3 denoting the three cams.
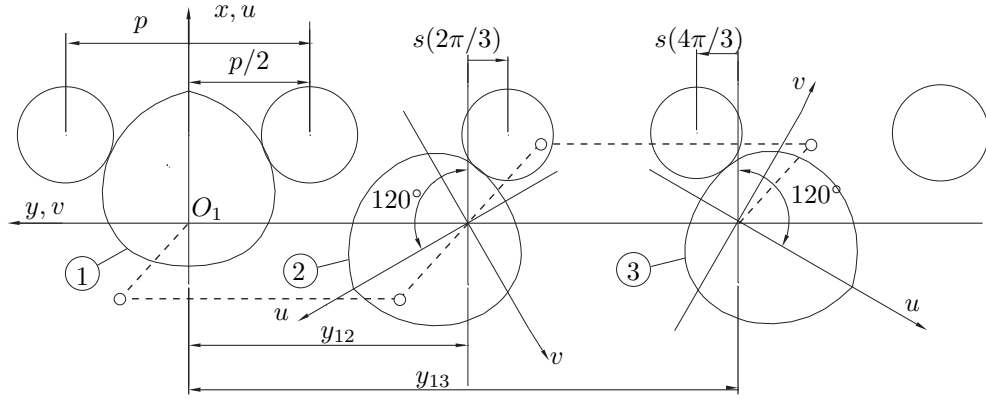

Figure 16: Layout of the non-coaxial conjugate-cam mechanism on three parallel shafts

The profile of each cam is as described in Section 2. The cams are mounted in such a way that the angle between the u-axis of cams 1 and 2 is 120°, while the angle between the u-axis of cams 1 and 3 is 240°. According to the configuration of the mechanism depicted in Fig. 16, and denoting by y_{12} and y_{13} the distance between the origin of 1 and 2, and between the origin of 1 and 3, respectively, we have

$$y_{12} = p/2 + p + s(2\pi/3) , \quad y_{13} = p/2 + 2p + s(4\pi/3)$$

Using the expression of the input-output function s given in Eq. (1), we obtain

$$y_{12} = 4p/3 , \quad y_{13} = 8p/3 \tag{43}$$

Figure 17 shows the pressure angle variation for each cam vs. ψ, where *1*, *2* and *3* denote the plot of the pressure angle for cams 1, 2 and 3, respectively. Moreover, cams *2* and *3* are rotated by angles $2\pi/3$ and $4\pi/3$, respectively, from cam *1*. We can also consider that the plot for cam 3 that drives the follower before cam 1 in a previous cycle, referred to as *3'* in Fig. 17, is out of phase $-2\pi/3$ with respect to cam *1*. As we saw in Eq. (14), cam 1 can drive the follower within $\pi \leq \psi \leq 2\pi - \Delta$, which corresponds in Fig. 17 to the part of the plot *1* between points B and D.

Consequently, cam 2 can drive the follower within

$$\pi + 2\pi/3 \leq \quad \psi \quad \leq 2\pi - \Delta + 2\pi/3 \quad i.e. \quad 5\pi/3 \leq \psi \leq 8\pi/3 - \Delta$$

and cam 3 within

$$\pi + 4\pi/3 \leq \quad \psi \quad \leq 2\pi - \Delta + 4\pi/3 \quad i.e. \quad 7\pi/3 \leq \psi \leq 10\pi/3 - \Delta$$

which is equivalent to saying that cam 3 can drive the follower in a previous cycle, within

$$\pi - 2\pi/3 \leq \quad \psi \quad \leq 2\pi - \Delta - 2\pi/3 \quad i.e. \quad \pi/3 \leq \psi \leq 4\pi/3 - \Delta$$

The above interval corresponds in Fig. 17 to the part of the plot *3'* between points A and C. Consequently, there is a common part for cams 1 (plot *1*) and 3 (plot *3'*) during which these two cams drive the follower, namely, between points B and C, which corresponds to

$$\pi \leq \psi \leq 4\pi/3 - \Delta \tag{44}$$

Moreover, during this common part, cam 3 has lower absolute pressure angle values than cam 1, and hence, we consider that only cam 3 drives the follower. Consequently, cam 1 drives the follower only within

η	a_4 (mm)	a_5 (mm)	$v_{L\max}$ (μm)	$|\mu_{\min}|$ (°)	$|\mu_{\max}|$ (°)	service factor (%)
0.5	15.5	6.56	0.26	28.59	49.41	10.49
0.4	10.5	3.44	2.88	20.31	37.20	70.02
0.39	10	3.12	4.14	19.46	35.81	76.02
0.38	9.5	2.81	6.20	18.61	34.39	82.02
0.37	9	2.50	9.76	17.75	32.95	88.03
0.36	8.5	2.19	16.39	16.89	31.48	94.04
0.35	8	1.87	29.89	16.03	29.98	100
0.34	7.5	1.56	61.07	15.17	28.47	100
0.33	7	1.25	147.02	14.31	26.93	100
$1/\pi$	6.41	0.88	576.95	13.31	25.12	100

Table 2: Design parameters, roller pin deformation and pressure angle for the novel conjugate-cam mechanism of Fig. 15, with $p = 50$ mm, $b = 9.5$ mm, $L = 10$ mm, $\tau = 1.2$ Nm and $E = 2 \times 10^5$ MPa.

$4\pi/3 - \Delta \le \psi \le 2\pi - \Delta$. These boundaries allow us to have a pressure angle lower than with coaxial conjugate cams, since we do not use anymore the part of the cam profile within $\pi - \Delta \le \psi \le 4\pi/3 - \Delta$, which has high absolute pressure angle values. We can thus obtain a higher service factor for the mechanism.

The maximum roller-pin deformation $v_{L\max}$ derived in eq.(42) is reasonably low. In Table 2, we record the values of η, a_4, a_5, $v_{L\max}$, $|\mu_{\min}|$, $|\mu_{\max}|$ and the service factor for the three-conjugate-cam mechanism of Fig. 15. The best compromise is to use the three-conjugate-cam mechanism with $\eta = 0.37$, whence the radius of the roller is $a_4 = 9$ mm and the roller-pin deformation is $v_{L\max} = 9.76$ μm with a good service factor of 88.03%.

6   Conclusions

The optimum design of Slide-o-Cam was made for two types of mechanism, i.e. with two and three-conjugate-cams. The three-conjugate-cam mechanism reported here allows us to drive the Orthoglide with prismatic actuators using rotary DC motors. Moreover, the roller-pin deformation is minimized, and the service factor is substantially increased with respect to the layout of Fig. 14. Further research is currently underway to evaluate the influence of the number of lobes on each cam to increase the service factor using only two cams.

References

[1] González-Palacios, M. A. and Angeles, J., 2003, The design of a novel pure-rolling transmission to convert rotational into translational motion", *ASME Journal of Mechanical Design*, Vol. 125, pp. 205-207
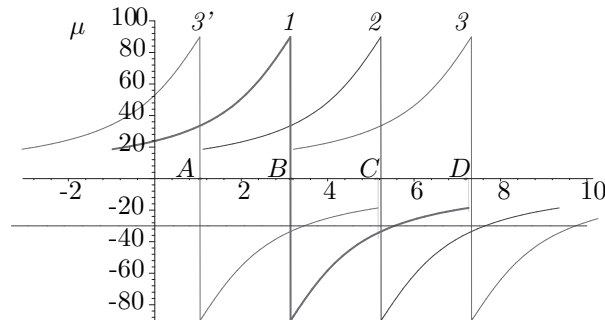

Figure 17: Pressure angle for the three cams

[2] Chablat, D. and Wenger Ph. 2003, "Architecture Optimization of a 3-DOF Parallel Mechanism for Machining Applications, the Orthoglide," *IEEE Transactions on Robotics and Automation*, Vol. 19/3, pp. 403-410, June.

[3] Lampinen, J., 2003, "Cam shape optimisation by genetic algorithm," *Computer-Aided Design*, Vol. 35, pp. 727-737.

[4] Zhang, Y. and Shin, J.-H., 2004, "A Computational Approach to Profile Generation of Planar Cam Mechanisms," *ASME Journal of Mechanical Design*, Vol. 126-1, pp. 183–188.

[5] Bouzakis, K.D., Mitsi, S. and Tsiafis, J., 1997, "Computer-Aided Optimum Design and NC Milling of Planar Cam Mechanims," *Int. J. Math. Tools Manufact.*, Vol. 37, No. 8, pp. 1131-1142.

[6] Carra, S., Garziera, R. and Pellegrini, M., 2004, "Synthesis of cams with negative radius follower and evaluation of the pressure angles," *Mechanism and Machine Theory*, Vol. 34, pp. 1017–1032.

[7] González-Palacios, M. A. and Angeles, J., 1993, *Cam Synthesis*, Kluwer Academic Publishers B.V., Dordrecht.

[8] Waldron, K. J. and Kinzel, G. L., 1999, *Kinematics, Dynamics, and Design of Machinery*, John Wiley & Sons, Inc., New York.

[9] Lee, M.K., 2001, *Design for Manufacturability of Speed-Reduction Cam Mechanisms*, M.Eng. Thesis, Dept. of Mechanical Engineering, McGill University, Montreal.

[10] Angeles, J. and López-Cajún,C., 1991, *Optimization of Cam Mechanisms*, Kluwer Academic Publishers B.V., Dordrecht.

[11] Teng, C.P. and Angeles, J., 2004, "An optimality criterion for the structural optimization of machine element," *ASME Journal of Mechanical Design*, Accepted for publication.

[12] Renotte, J. and Angeles, J. 2003, "The Design of a Pure-Rolling Cam Mechanism to Convert Rotationnal into Translational Motion," Department of Mechanical Engineering and Centre for Intelligent Machines Report, TR-CIM-03-06, August, McGil University, Montreal.